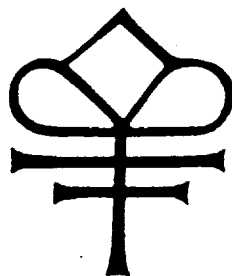


# APPENDIX C



**N 9 3 - 1 5 5 9 2**

**Liquid Xenon Time Projection Chamber  
for Gamma Rays in the MeV Region: Development Status**

E. Aprile, A. Bolotnikov, D. Chen and R. Mukherjee  
Department of Physics and  
Columbia Astrophysics Laboratory, Columbia University  
538 West 120th Street, New York, NY 10027, USA

Presented at the: "*Gamma-Ray Detectors*"  
Conference of the SPIE's International Symposium  
on Optical Engineering, 19 -24 July 1992

**COLUMBIA UNIVERSITY**  
DEPARTMENTS OF  
**PHYSICS and ASTRONOMY**  
NEW YORK, NEW YORK 10027

Liquid Xenon Time Projection Chamber  
for Gamma Rays in the MeV Region: Development Status

E. Aprile, A. Bolotnikov, D. Chen and R. Mukherjee

Dept. of Physics and  
Columbia Astrophysics Laboratory  
Columbia University, New York NY 10027

ABSTRACT

The feasibility of a large volume Liquid Xenon Time Projection Chamber (LXe-TPC) for three-dimensional imaging and spectroscopy of cosmic gamma-ray sources, was tested with a 3.5 liter prototype. The observation of induction signals produced by MeV gamma-rays in liquid xenon is reported, with a good signal-to-noise ratio. The results represent the first experimental demonstration with a liquid xenon ionization chamber of a non-destructive read-out of the electron image produced by point-like charges, using a sense wire configuration of the type originally proposed in 1970 by Gatti et al. An energy resolution as good as that previously measured by us with millimeter size chambers, was achieved with the large prototype of 4.4 cm drift gap.

1. INTRODUCTION

Liquid xenon (LXe) is a very attractive medium for  $\gamma$ -ray detectors, because of its excellent combination of: high atomic number ( $Z=54$ ), high density ( $3.06 \text{ gcm}^{-3}$ ), low  $W$ -value (15.6 eV), small Fano factor (0.04), small diffusion coefficient ( $65 \text{ cm}^2\text{s}^{-1}$ ), and high electron mobility ( $> 2000 \text{ cm}^2\text{s}^{-1}\text{V}^{-1}$ ). When used in an ionization chamber operated in the time projection mode (TPC), this medium combines high detection efficiency, excellent spatial resolution, very good energy resolution, and superior background identification and rejection ability. Thus, a LXe-TPC offers an unique potential for spectroscopy and imaging of cosmic  $\gamma$ -ray sources with high sensitivity and good angular resolution. The continuing emphasis of our research program has been to demonstrate the feasibility of high resolution liquid xenon imaging detectors in the field of  $\gamma$ -ray astrophysics. In the energy range from  $\sim 100$  keV to  $\sim 30$  MeV future advances require at least arcminute angular resolution and flux sensitivity for  $\gamma$ -ray lines (e.g. MeV) at the level of  $10^{-6} \text{ photons cm}^{-2} \text{ s}^{-1}$ . Following these considerations, two  $\gamma$ -ray telescope designs based on a LXe-TPC tailored to a specific energy range and scientific program, emerged from our studies.

The first one is optimized for the few MeV energy region. It uses a LXe-TPC with 10 cm drift gap and  $1200 \text{ cm}^2$  sensitive area, with millimeter spatial resolution requirement. By combining the 3-D position sensitive LXe  $\gamma$ -ray detector with a coded aperture mask at a separation of 1 meter, an angular resolution better than  $0.5^\circ$  can be achieved over the entire energy range 0.3–10 MeV. The unique capability of the LXe detector to use Compton kinematics to reject background events as well to measure polarization of MeV  $\gamma$ -rays with high sensitivity is emphasized for this version of a LXe-TPC telescope, which we plan to test in the near space environment as a balloon-borne payload. The study of two of the most pressing problems in low energy  $\gamma$ -ray astronomy, namely the determination of the actual source distribution of the 0.511 MeV positron-electron annihilation line and of the 1.809 MeV  $^{26}\text{Al}$  line, will be the main scientific objective.<sup>1,2</sup>

The second telescope consists of a LXe-TPC with a larger sensitive volume ( $> 30$  liters) and superior spatial resolution, optimized for the 1 – 30 MeV energy region where Compton scattering and pair production are the dominant  $\gamma$ -ray interaction processes. In a Compton telescope, the true direction of the  $\gamma$ -ray source can only be unambiguously identified when the direction of the Compton scattered electrons or electron-positron pairs are accurately measured. In the dense liquid xenon, the range of these electrons is very short (of the order of millimeters) so that a spatial resolution of a few hundred microns is required.<sup>3</sup>

There are many technical challenges to the construction of the LXe-TPC for these  $\gamma$ -ray telescopes. The most fundamental one is the purity of the liquid, which has to be at the ppb level to permit the drift of ionization electrons

over large distances. This problem has already been extensively studied and solved by us.<sup>4</sup> The second very important problem is the implementation of a non-destructive readout of the electronic signals to realize the 3-D imaging of any ionizing event in the sensitive volume. We report here, for the first time, the initial results from a study of the imaging performance of a 3.5 liter LXe-TPC as  $\gamma$ -ray detector. The equally important issue of good energy resolution in a large volume liquid xenon detector was also studied with this prototype and the results are presented here. These results are the first experimental evidence of the feasibility of a LXe detector of practical size and of its capability for good calorimetry and imaging.

## 2. LXe-TPC PROTOTYPE

The technical challenges of a liquid xenon detector for  $\gamma$ -rays were addressed with the development of a 3.5 liter prototype, shown schematically in Fig. 1. The detector is a large volume gridded ionization chamber with a maximum drift gap of 6.0 cm, compared to the 10 cm of the proposed LXe-TPC telescope. The active volume is defined by the cathode plate, the shielding grid and a sequence of equally spaced shaping rings which ensure the uniformity of the electric field for the drift of the electrons. The total active volume of  $\sim 365 \text{ cm}^3$  ( $7.8 \text{ cm} \times 7.8 \text{ cm} \times 6.0 \text{ cm}$ ), is much larger than the size of the typical liquid xenon ionization chambers reported in the literature so far. To irradiate the liquid xenon with  $\gamma$ -rays, a  $^{207}\text{Bi}$  source is placed on the cathode plate, facing away from the active volume. Radiation entering the active volume has to first pass through 3 mm of stainless steel. This effectively blocks all conversion electrons from the  $^{207}\text{Bi}$  so that the detector is sensitive only to  $\gamma$ -ray interactions.

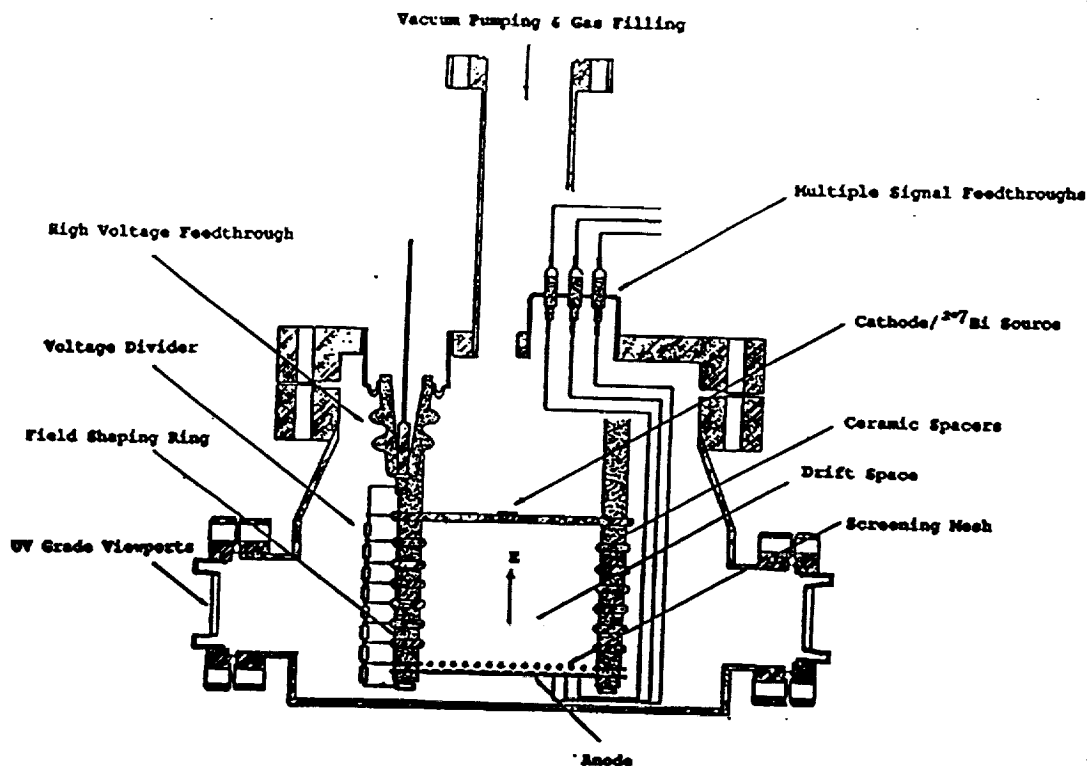


Fig. 1. The 3.5 liter LXe-TPC prototype  $\gamma$ -ray telescope.

To study the energy resolution, a single charge collector was placed 7 mm behind the shielding grid. The grid is actually a mesh made of nickel, with 0.8 mm spacing and  $50 \mu\text{m}$  wire width spot-welded on a stainless steel frame. The field strengths on the two sides of the mesh have to be optimized to obtain a maximum shielding efficiency and transparency for the drifting electrons. The critical field ratio of 1.75, was calculated by the formula given by Bunemann et al.,<sup>5</sup> modified for a mesh type grid. This value was verified experimentally. During the operation of the detector a field ratio of 2 was typically chosen. A custom built low noise, charge sensitive preamplifier was used

to detect the signals from the collector plate. To allow the observations of slow rising signals, the decay time of the amplifier was set to 1 ms. To reduce the input capacitance, the amplifier was mounted as close as technically feasible to the signal feed-through.

To study the spatial resolution the chamber structure was modified into a 2-D TPC, with the electrode geometry shown schematically in Fig. 2. The same cathode plate with the radioactive source was used for these experiments. The shielding mesh was replaced by a plane of equally spaced wires with a pitch of 2 mm. Between this grid and the collector plate, a plane of sense wires, with the same 2 mm pitch, was introduced for the detection of the induction signals. The induction plane was at a distance of 2 mm from the shielding grid plane and 4 mm from the collector plate.

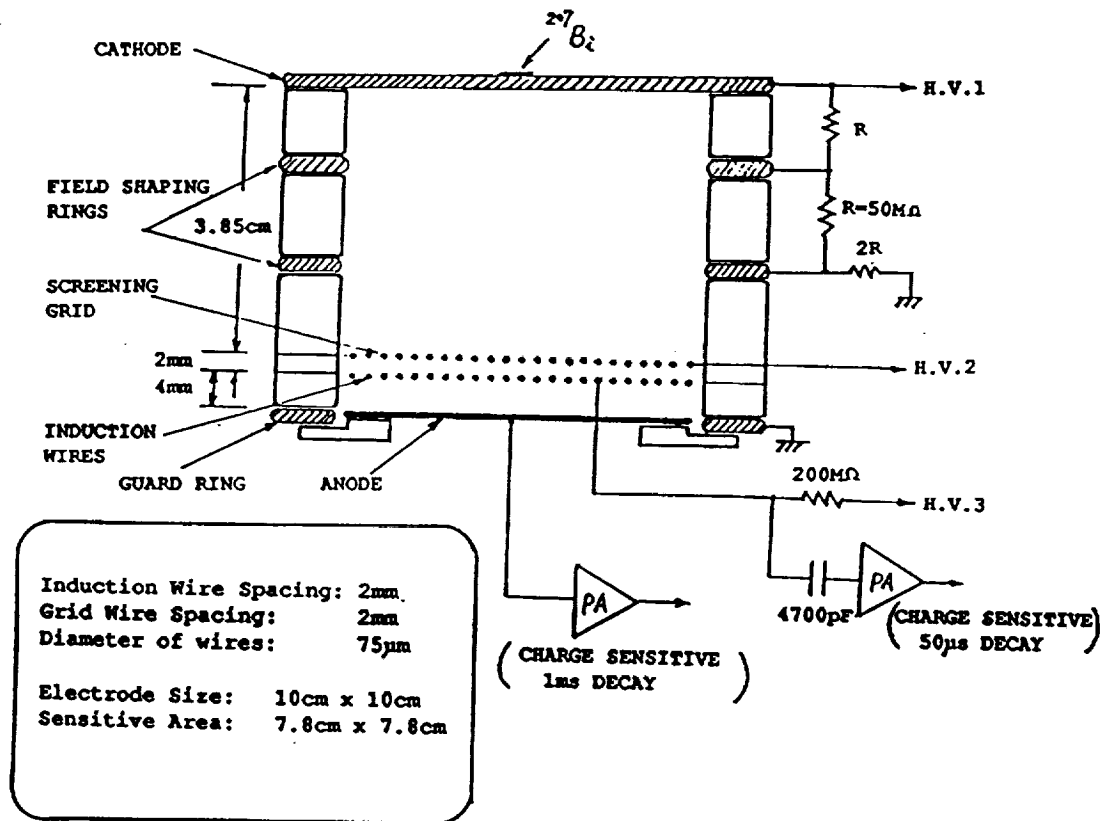


Fig. 2. Schematic of the 2-D LXe-TPC electrode structure for the measurement of the induction signals.

This electrode arrangement provides the two coordinates for the position of each point of interaction, one coordinate being determined by the drift time and the other by the position of the sense wire. For a non-destructive readout of the electron image on the induction wires, the electric field between the induction and the collection planes has to be correctly chosen so as to allow the field lines to pass between the sense wires. The right potentials for this condition were calculated and the field map is shown in Fig. 3.

The sense wires are biased with their "natural" potential in order not to distort the field distribution. The induction signal on each wire is detected with a low noise charge sensitive preamplifier, via a decoupling capacitor. Due to the fast rise time of these signals a decay time of 50 μs was used. The total number of sense wires read-out was 20. The output of each preamplifier was connected to a FADC through an additional amplification stage.

To purify the xenon gas needed to fill the 3.5 liter volume, we used the purification system shown in Fig. 4. This is essentially a larger scale version of the purification system previously used for liquid xenon chambers.

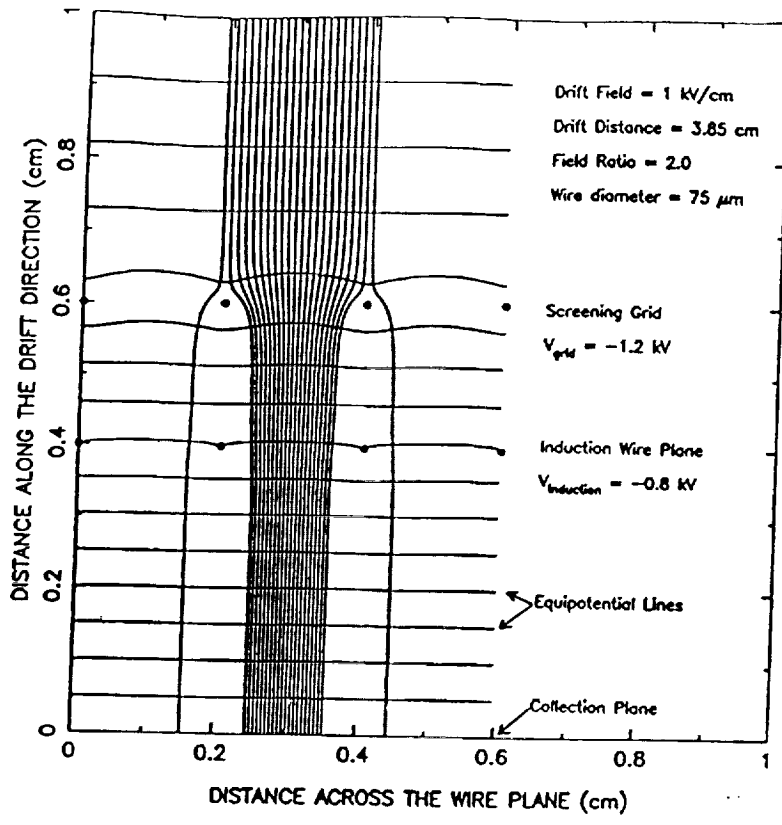


Fig. 3. The electric field map of the 2-D LXe TPC of Fig. 2.

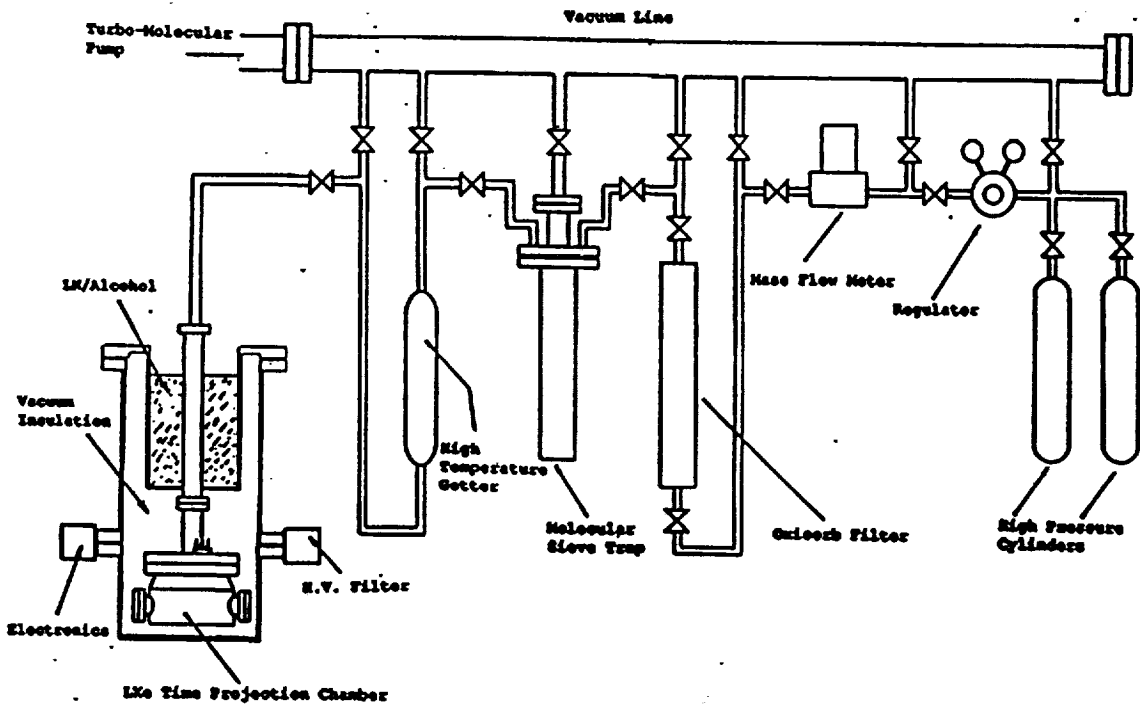


Fig. 4. The xenon gas purification system.

The system uses a combination of Oxisorb, cold molecular sieves, and high temperature getters, to effectively reduce electronegative impurities from commercial xenon gas, to less than 1 ppb. Details on the design and performance of our system can be found in an earlier publication.<sup>4</sup> To maintain the purity of the liquid, special care is paid in the preparation of the detector vessel and internal structure, as well as any other material in contact with the gas or the liquid. Pre-cooling of the xenon gas was achieved by surrounding a long filling pipe on top of the chamber vessel by a liquid nitrogen bath. Once the chamber vessel was full, an operating liquid temperature of about  $-100^{\circ}\text{C}$  was easily maintained by a mixture of liquid nitrogen and ethyl alcohol.

### 3. EXPERIMENTAL RESULTS

#### 3.1. Energy Resolution Performance

Figure 5 shows the typical output signals of the charge sensitive preamplifier. The steps in the signals clearly indicate the different ionization processes, produced by the  $^{207}\text{Bi}$   $\gamma$ -ray interactions inside the LXe sensitive volume. For a gridded ionization chamber, the induced charge signal starts once the electrons pass the shielding mesh and linearly increases as the electrons move towards the collector. Since the decay time constant of the amplifier is much longer than the drift time, the pulse height appears to be constant after a step. The rise time of a single step is about  $2.5 \mu\text{s}$ , which corresponds directly to the drift time between mesh and anode. This is consistent with the signal produced by a point like charge, as expected by the short range (much less than 1 mm) of low energy electrons in liquid xenon. This results in the unique feature of a liquid xenon ionization chamber to visualize the multiple-site energy depositions produced by the interactions of MeV  $\gamma$ -rays. Figure 5 clearly demonstrates this feature. The single step signal is due to a photoelectric interaction (Fig. 5 a). The multi-step signals are due to multiple-site interactions produced by one or more Compton scatterings followed by a photoelectric absorption (Fig. 5 b,c).

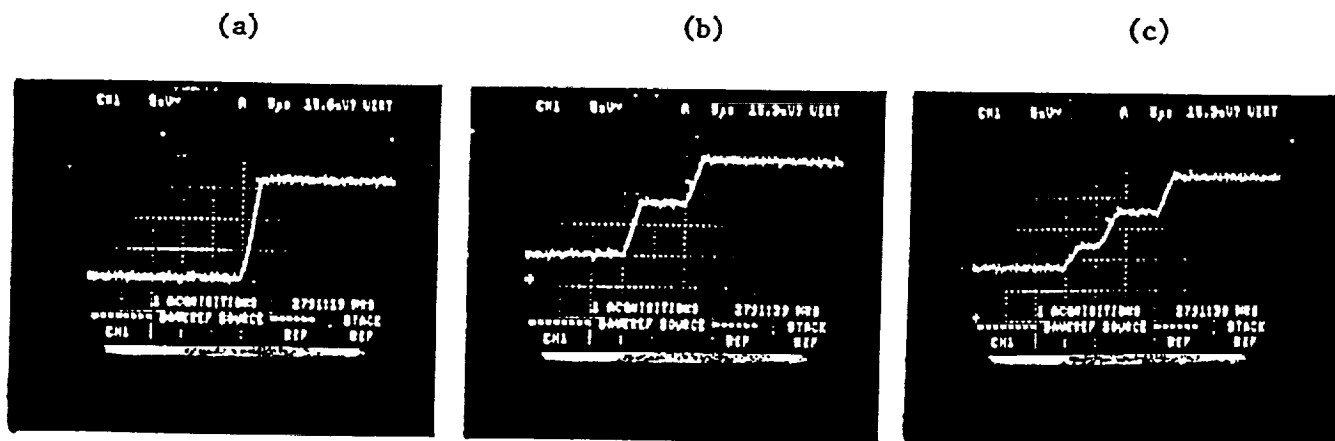


Fig. 5. Ionization pulses from  $^{207}\text{Bi}$  1.77 MeV  $\gamma$ -ray interactions in the 3.5 liter LXe chamber. (a) Single photoabsorption event. (b, c) Multiple Compton scattering events, followed by a photoabsorption.

As we know, Compton interaction is dominant in the few MeV region. The larger the depth of the liquid xenon, the greater the fraction of multiple-site events which contribute to the full energy peak. Monte Carlo simulation shows that for a  $\gamma$ -ray of 1 MeV in 6.0 cm of LXe, more than 50% of the interactions are from multiple Compton scatterings. All these interactions are separated in time by the propagation of the photon, but within the time scale of the detector they are simultaneous. The observation of the signal, however, takes place only after the drift time in the active volume, which depends on the location of the interaction point. Therefore, these multiple-site events are observed as multi-step features in the pulse shape. The height of the step gives the energy deposited at the point of interaction, and the time intervals between the steps give the relative distances of the interaction points, along the drift direction. The sum of all the step pulse-heights is proportional to the energy of the original  $\gamma$ -ray, if totally

absorbed. For example, based on the calibration of the charge sensitive preamplifier, the energy of all three events shown in Fig. 5 corresponds to 1.77 MeV  $\gamma$ -rays from the  $^{207}\text{Bi}$  source. The information on the individual step pulse height and on the timing is very valuable. This timing, however, only gives information on the Z-coordinate of each site. By combining this with the additional information on the X-Y coordinates, event reconstruction based on Compton kinematics is possible as shown in reference. <sup>2</sup> This gives the capability of background identification and rejection. It also gives the capability to use a LXe-TPC as a Compton polarimeter of high sensitivity in the MeV energy range.

The overall energy resolution  $\Delta E_t$  of the detector can be expressed as a combination of the following terms: the fluctuation in the number of electron-ion pairs produced  $\Delta E_f$ , the electronic noise  $\Delta E_e$ , the grid shielding inefficiency  $\Delta E_s$ , the fluctuation in the collected charge due to recombination  $\Delta E_r$ , and the variation of signal risetime  $\Delta E_b$ . The full width at half maximum of the energy resolution can then be expressed as follows:

$$\Delta E_t^2 = \Delta E_f^2 + \Delta E_e^2 + \Delta E_s^2 + \Delta E_r^2 + \Delta E_b^2 \quad (1)$$

The fluctuation of the electron-ion pairs is theoretically predicted as,  $\Delta E_f^2 = (2.35)^2 FWE$  where  $W$  is the average energy required to create one electron-ion pair,  $F$  is the Fano factor, and  $E$  is the energy of the ionizing particle. The magnitude is about 0.2% FWHM at 1 MeV, a value which was experimentally never reached. The best observed value was 6% at 0.57 MeV. <sup>6</sup> An interpretation of the large discrepancy is given elsewhere. <sup>6</sup>

The contribution from the electronic noise can be measured directly from the test pulse distribution. The typical noise contribution in our system is about 24 keV FWHM.

The grid shielding inefficiency contribution is estimated to be smaller than 1%.

The contribution of ballistic deficit, due to pulse rise time variation, is significant only in large volume detectors and can be minimized by appropriate signal processing.

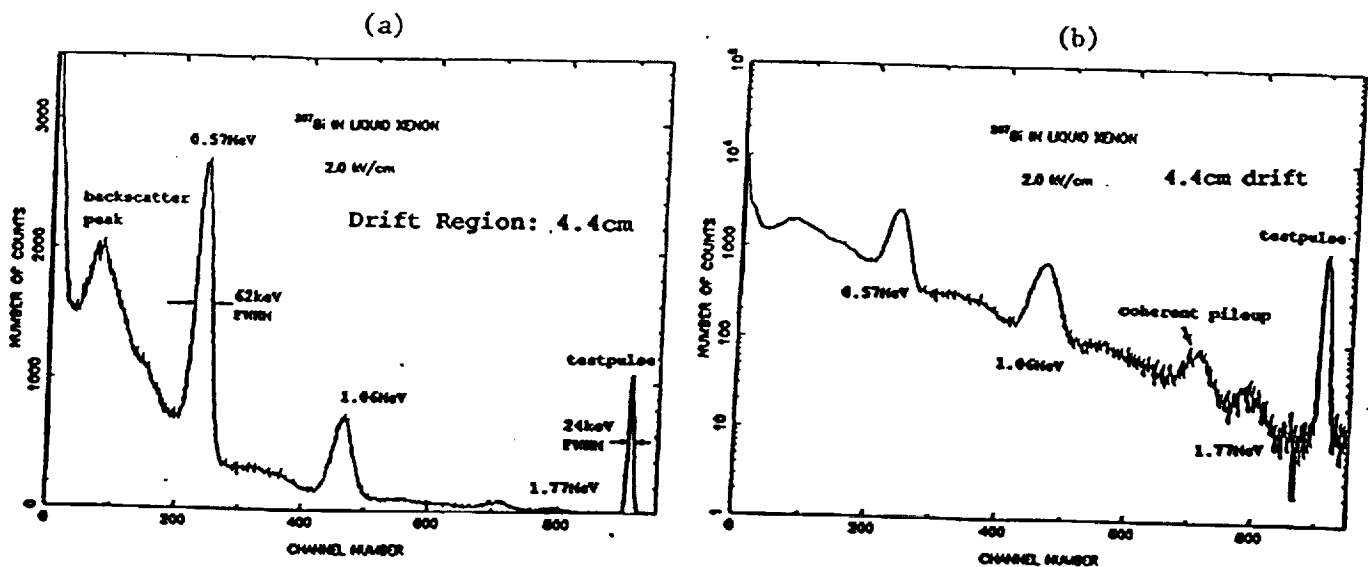


Fig. 6. (a)  $^{207}\text{Bi}$   $\gamma$ -ray spectrum recorded at 2 kV/cm with the 3.5 liter LXe chamber of 4.4 cm drift gap. (b) Same spectrum as that of Fig. 6a in semi-logarithmic scale.

In the case of a long drift LXe ionization chamber, the charge collection time can vary by more than 20  $\mu\text{s}$  due to the multiple-site events. To completely collect all the charge, long shaping times are therefore required. This seriously reduces the speed of the detector, and also makes the measurement more sensitive to low frequency noise. Two solutions to the problem of ballistic deficit are: a) A gated integrator determining the total pulse height on-line. b) Waveform digitization and off-line reconstruction of the pulses.

The gated integrator solution is insensitive to rise time variations, as pointed out by Radeka. <sup>7</sup>

Fig. 6a shows the  $^{207}\text{Bi}$  spectrum in the 3.5 liter chamber, obtained with a multi-channel analyzer after a  $2\ \mu\text{s}$  unipolar shaping of the signal, followed by a  $2\ \mu\text{s}$  gated integrator. Fig. 6b is the same spectrum in a semi-logarithmic scale. This spectrum was obtained with the drift gap reduced from 6.0 cm to 4.4 cm, in order to operate the chamber at high drift fields without voltage breakdown problems. The spectrum can be compared with that obtained earlier with much smaller chambers<sup>6</sup> where the maximum drift was few millimeters. The electronic noise subtracted energy resolution is compared in Fig. 7. Two important remarks can be made:

- (a) The noise subtracted energy resolution of the large chamber is 10% at 0.57 MeV, comparable to that in the small chamber, at the same drift field. This means that fluctuation in the recombination process is the dominant factor of Eq. (1) which determines the measured resolution. It also means that the liquid purity was sufficient for long drift and that the signal processing with the gated integrator did not affect the resolution.
- (b) Several peaks in the spectrum can only be observed in the large chamber due to its increased detection efficiency at high energies. Such features are the 1.77 MeV  $\gamma$ -rays, and the backscatter peak. A further feature is the peak at 1.63 MeV which is caused by 2 correlated events, i.e. a 0.57 MeV and a 1.06 MeV  $\gamma$ -ray emitted from the source simultaneously.

The gated integrator, however, reduces the detection efficiency, especially for high energy events, and also only conserves the total pulse height. The amplitude of each single step is lost. As previously mentioned, for a complete reconstruction of the event, the pulse height and position of each individual charge cloud are needed. These problems can be overcome by using a waveform digitizer on the anode without shaping of the original charge signal. Work on this method is under progress.

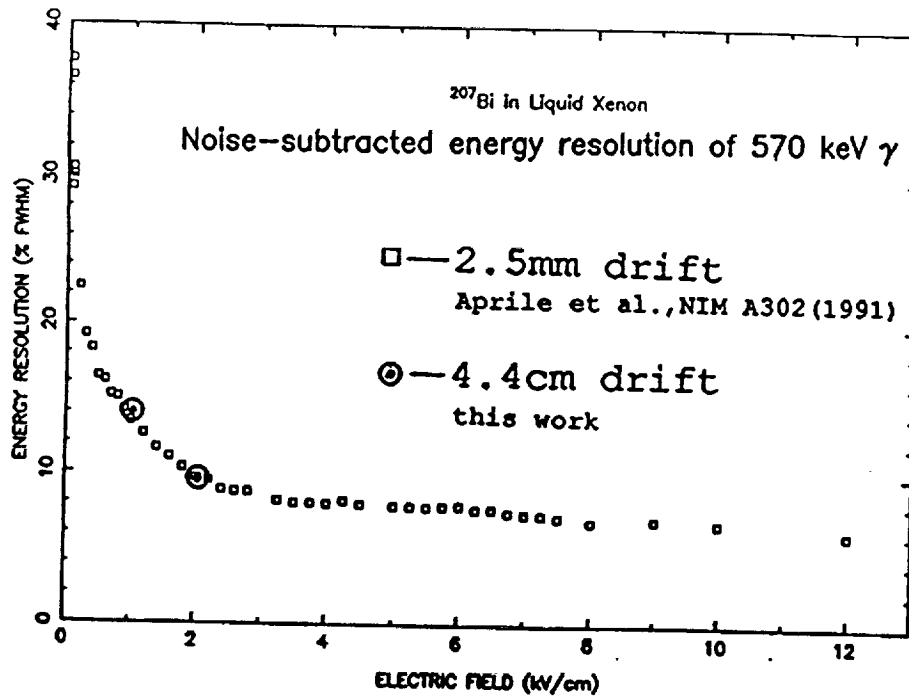


Fig. 7. Comparison of the noise-subtracted energy resolution of 570 keV  $\gamma$ -rays in LXe for 4.4 cm and 2.5 mm drift chambers.

### 3.2. Position Resolution Performance

The 3-D position resolution performance of a liquid xenon detector is largely determined by the read-out structure which is used to detect the signals induced by an ionizing event. In its simplest version, a system of two orthogonal



induction wire planes, separated from the drift region by a shielding grid, is used. The induced signals on the wires provide the X-Y information. The measured drift time, referred to a time zero, together with the known drift velocity, provides the Z-information. A single collection plate below the induction wires can be used for total charge collection. A preliminary design of the sensing electrodes geometry for 3-D imaging in a LXe-TPC as  $\gamma$ -ray telescope is shown in Fig. 8.

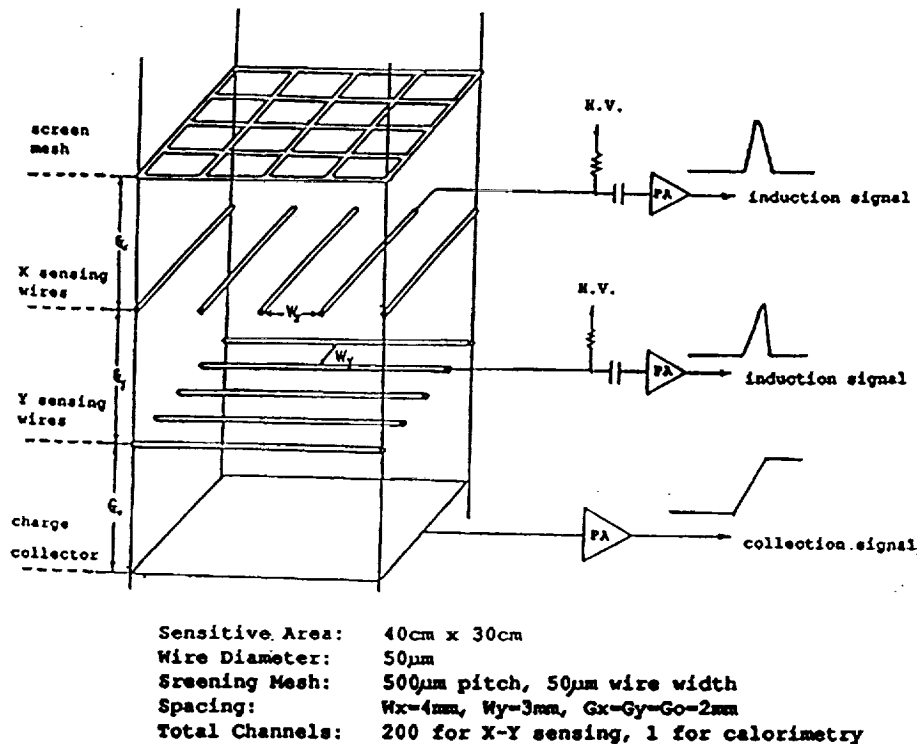


Fig. 8. Schematic of the 3-D LXe-TPC electrode structure.

The time zero to the readout will be provided by the primary scintillation light signal<sup>8</sup> produced within a few nsec of the  $\gamma$ -ray interaction. This design is based on the original one by Gatti et al.<sup>9</sup> These authors calculated the induced waveforms for this type of readout structure and showed (Fig. 9) that the amplitude of the signal produced by a point-like ionization depends strongly on the initial lateral position of the cloud between the sense wires. It was reported<sup>10</sup> that this effect is undesirable for tracking charged particles. For the gamma-ray application of a LXe-TPC, however, tracking capability is not needed since the density of the liquid is such that the small energy depositions produced by gamma-ray interactions result in localized or point-like charge blobs, in a detector with a practical wire spacing of the order of millimeters.

Actually this dependence of the induction signals on the position of the charge blobs with respect to the wires, can be an advantage for the spatial resolution. The location of a point charge can in fact be determined with a smaller error by weighing the signals from adjacent wires to obtain the center of gravity of the charge cloud. Without determining the center of gravity, the position of the cloud is determined from the location of the sense wire, and the error in localization of the cloud is  $s/\sqrt{12}$ , where  $s$  is the wire spacing. Using the signals from two adjacent wires to estimate the position reduces this error. Now the error is dominated by the accuracy of the amplitude measurement, i.e. the signal-to-noise ratio. Obviously, a smaller wire spacing still increases the position resolution, but cost and complexity considerations will limit the overall number of wires.

These considerations were tested with the 2-D 3.5 liter TPC prototype shown in Fig. 2, with the electric field lines as shown in Fig. 3. The first measurements were dedicated to the observation of the induction signal on the sense wires. Fig. 10 shows the induction signal produced by a  $^{207}\text{Bi}$   $\gamma$ -ray event, and the corresponding collection

signal recorded simultaneously.

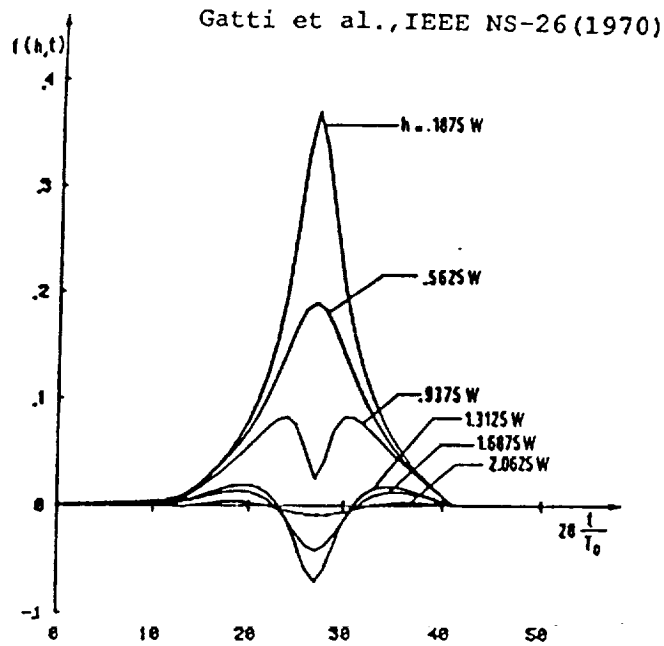


Fig. 9. The calculated induction waveform for a point-like charge at different lateral positions  $h$  from the sense wires spaced by  $W$ .

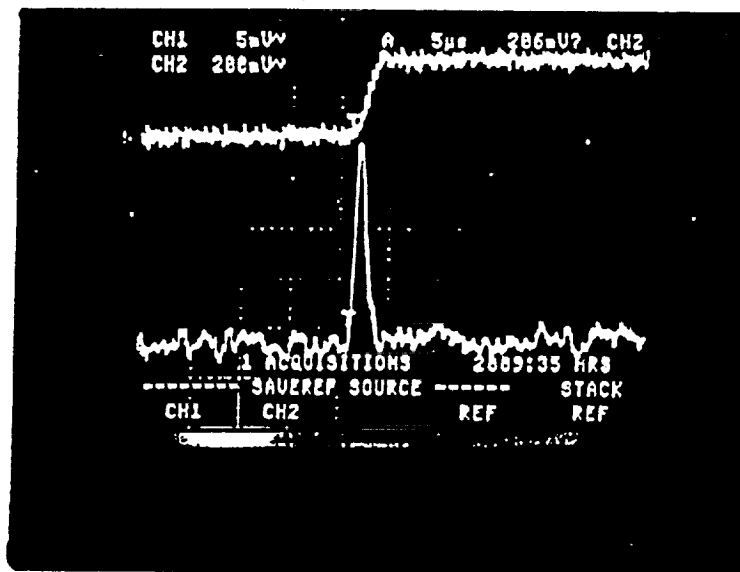


Fig. 10. Charge signal produced by a  $\gamma$ -ray event in the 2-D LXe-TPC. Upper trace: collection signal on anode (gain=1); Lower trace: induction signal on sense wire (gain=400).

The signal from the sense wire was used as the trigger. The induction signal was amplified by a gain of 400, while the gain of the collection signal was unity. For this event, the induced charge is  $\sim 30\%$  of the total collected charge, implying that the single  $\gamma$ -interaction point was close to the sense wire, based on Fig. 9. The induction signal has the same time duration as that of the collection signal, as expected. The induction signal has the expected triangular shape (see Fig. 9). It is not symmetric due to the shorter distance between the screening grid and the sense wires, than that between the sense wires and the collector. The signal-to-noise ratio is 12:1. This is sufficient

to significantly improve the position resolution inferred from the time information.

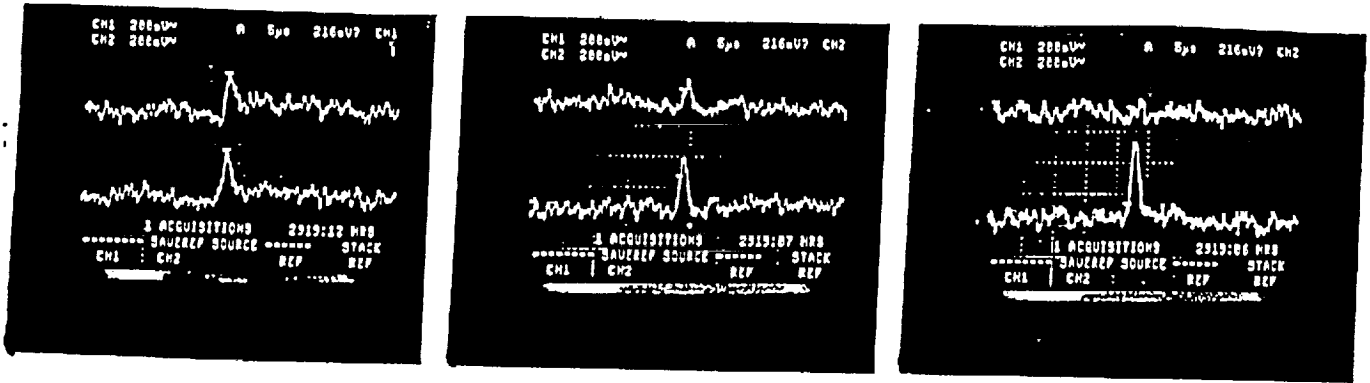


Fig. 11. Induced signals on neighboring wires observed in the 2-D LXe-TPC for different  $\gamma$ -ray events.

We also investigated the induction signals induced simultaneously on neighboring wires. As shown in Fig. 11, the relative amplitude of the signals changes on an event-by-event basis, indicating the different lateral positions of the charges produced by  $\gamma$ -ray interactions. This clearly demonstrates the potential to achieve a better spatial resolution on the X-Y coordinates than that determined by the wire spacing.

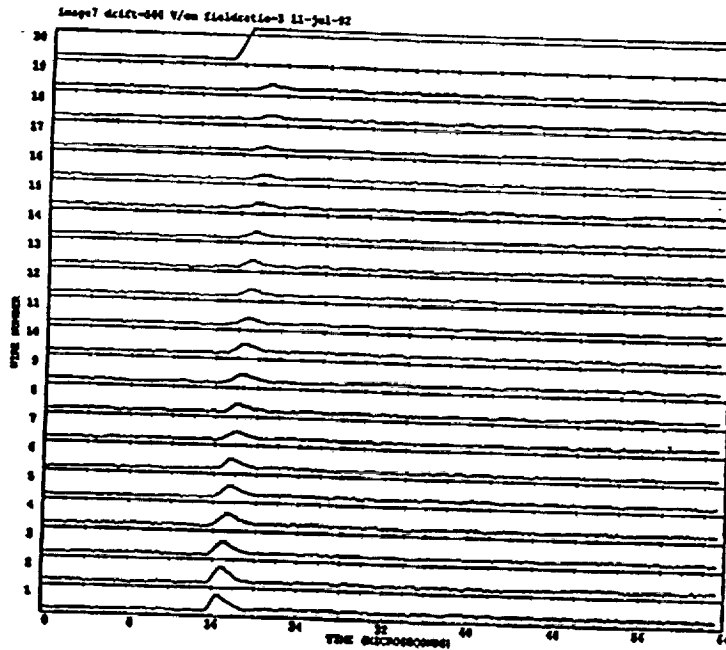


Fig. 12. Cosmic muon track observed with the 2-D LXe-TPC in induction mode.

Previously, the tracking capability of a 2D LXe-TPC was reported by using a segmented anode, read-out in collection mode.<sup>11</sup> With the present structure, charged particle tracks have been observed in the induction mode. Fig. 12 shows the signals induced on the sense wires by a cosmic muon passing through the chamber and depositing, successively, energy on all wires.

The signal from the anode, shown on channel 20 of Fig. 12, was used as the trigger. The timing of the signals

can be converted into drift length, and provides the coordinate of an ionizing event along the drift direction. Due to the triangular pulse shape, the determination of an accurate timing is easier than for the signal shape observed earlier in collection mode. This fact, together with the better signal to noise ratio, will improve the spatial resolution in this direction from the previously measured  $180 \mu\text{m}^{11}$ . The analysis of these data is still in progress. Intrinsically, the localization of the charge cloud is ultimately limited by electron diffusion along the drift path which causes a spread of the cloud. In the drift direction, a spatial resolution close to the diffusion limit can be expected. The final value depends on the accuracy on the timing of the pulses, limited in practice by the signal-to-noise ratio. The lateral diffusion, orthogonal to the drift direction, is given by  $\sqrt{Dt_d}$ , where  $D=65 \text{ cm}^2\text{s}^{-1}$  is the diffusion coefficient<sup>12</sup>,  $t_d$  is the drift time. For drift distances of maximum 10 cm, as in the proposed LXe-TPC telescope, the resulting value is negligible when compared with the spacing of the sense wires.

#### 4. CONCLUSION

A  $\gamma$ -ray telescope for the energy range from 0.3 MeV to 10 MeV was proposed to measure the  $\gamma$ -ray flux from galactic sources in balloon borne experiments. The telescope is based on a LXe-TPC as 3-D position sensitive detector and spectrometer, coupled to a coded aperture mask. The active area is  $1200 \text{ cm}^2$  and the maximum drift length 10 cm. The size of this TPC is considerably larger than liquid xenon detectors tested so far. To achieve the desired performance of the telescope, it is mandatory to measure the energy and position of all  $\gamma$ -ray interaction points produced by multiple Compton scatterings.

To evaluate the feasibility, a 3.5 liter prototype was constructed and repeatedly operated. The required purity level for the xenon gas was achieved with a simple purification system, of the type used for previous measurements with liquid xenon small volume detectors.

The prototype was tested in a gridded chamber configuration with 4.4 cm drift gap, for charge collection and energy resolution studies. With this large sensitive volume detector, the enhanced detection efficiency of liquid xenon for  $\gamma$ -rays is clearly visible. Despite the much longer drift distance, the noise-subtracted energy resolution measured with this detector is comparable, at the same electric field of 1 and 2 kV/cm, to that previously measured with smaller size chambers.

The feasibility of a non-destructive electron imaging of ionization events with a liquid xenon TPC was established. For this purpose, the readout structure consisted of an induction plane of sense wires to provide the position information and a collector plate for total charge collection. The induced signals produced by MeV  $\gamma$ -rays and cosmic ray muon tracks on sense wires have been observed, for the first time, in liquid xenon. A large signal-to-noise ratio was achieved and the pulse shape and timing of the induction signals were consistent with expectation. For the final detector, a position resolution better than  $s/\sqrt{12}$  can be expected, where  $s$  is the wire spacing. Along the drift direction, the resolution will be better than  $180 \mu\text{m}$  measured earlier, since a more accurate timing is possible on the induced waveforms, and due to the improved signal to noise ratio.

#### 5. ACKNOWLEDGEMENTS

This work was supported by NASA grant NAGW-2013 and partially by NSF grant PHY-91-09937. We also would like to thank many colleagues, and in particular D. Schinzel, V. Radeka, S. Rescia and F. Pietropaolo for support and valuable discussions.

#### 6. REFERENCES

1. E. Aprile et al., "A High Resolution Liquid Xenon Imaging Telescope for 0.3 – 10 MeV Gamma-Ray Astrophysics: Construction and Initial Balloon Flights," NASA proposal, CAL-2015 (1992).
2. E. Aprile et al., "A Monte Carlo Analysis of the Liquid Xenon TPC as Gamma-Ray Telescope," to be published in *Nucl. Instr. and Meth. A* (Aug.1992).

3. E. Aprile, R. Mukherjee, and M. Suzuki, "EUV, X-Ray and Gamma-Ray Instrumentation for Astronomy and Atomic Physics," *SPIE Conference Proceedings*, ed.C.J. Hailey and O.H.W. Siegmund, 1159, (1989) 295.
4. E. Aprile, R. Mukherjee and M. Suzuki, *Nucl. Instr. and Meth.*, A300, (1991) 343.
5. O. Bunemann, T.E. Cranshaw and I.A. Harvey, *Can. J. of Res.*, 27 (1947) 191.
6. E. Aprile, R. Mukherjee and M. Suzuki, *Nucl. Instr. and Meth.*, A302 (1991) 177.
7. V. Radeka, *Nucl. Instr. and Meth.*, 99 (1972) 525.
8. E. Aprile, R. Mukherjee and M. Suzuki, *IEEE Trans. Nucl. Sci.*, NS-37, (1990) 553.
9. E. Gatti et al., *IEEE Trans. Nucl. Sci.*, NS-26, (1970) 2910.
10. E. Bonetti et al., *Nucl. Instr. and Meth.*, A286 (1990) 135.
11. E. Aprile et al., *Nucl. Instr. and Meth.*, A316, (1992) 29.
12. E. Shibamura, et al., *Phys. Rev.*, A20, (1979) 2547.